microbiology research

MDPI

Article

Biosynthesis of Zinc Oxide Nanoparticles Using Garlic Peel Extract and Their Antibacterial Potential

Ali Abdelmoteleb [1], Benjamín Valdez-Salas [2], Ernesto Beltran-Partida [2], Vianey Mendez-Trujillo [3], Daniel González-Mendoza [4,*], Olivia Tzintzun-Camacho [4] and Ahmed F. Roumia [5]

[1] Botany Department, Faculty of Agriculture, Menoufia University, Shibin El-Kom 32514, Egypt; ali.abdelmoteleb4@agr.menofia.edu.eg
[2] Institute of Engineering, Autonomous University of Baja California, Calle de La Normal S/N and Boulevard Benito Juárez, Mexicali 21100, Mexico; benval@uabc.edu.mx (B.V.-S.); beltrane@uabc.edu.mx (E.B.-P.)
[3] Faculty of Medicine, Autonomous University of Baja California, Dr. Humberto Torres Sanginés S/N, Centro Cívico, Mexicali 21000, Mexico; vianey.mendez.trujillo@uabc.edu.mx
[4] Institute of Agricultural Sciences, Autonomous University of Baja California, Carretera a Delta s/n, Ejido Nuevo Leon, Mexicali 21705, Mexico; otzintzun@uabc.edu.mx
[5] Department of Agricultural Biochemistry, Faculty of Agriculture, Menoufia University, Shibin El-Kom 32514, Egypt; ahmed.fouad95@agr.menofia.edu.eg
* Correspondence: danielg@uabc.edu.mx

Abstract: Zinc oxide nanoparticles (ZnO NPs) have gathered interest because of their unique characteristics and potential applications. In the current work, ZnO NPs underwent an eco-friendly biosynthesis process using garlic peel extract. The biosynthesized ZnO NPs were characterized using different analyses including Ultraviolet-visible (UV-vis) spectroscopy, scanning electron microscopy (SEM), energy-dispersive X-ray spectroscopy (EDS), dynamic light scattering (DLS), and Fourier transform infrared spectroscopy (FTIR). The produced ZnO NPs exhibited a UV–vis spectrum absorption peak at 365 nm, thus indicating the formation of ZnO NPs. The SEM showed that the biosynthesized ZnO NPs had an irregular surface morphological shape with an average size of 17 nm, according to the DLS analysis. Based on the FTIR findings, the bioactive functional groups responsible for stabilizing and capping the ZnO-NPs were confirmed. The biosynthesized ZnO NPs exhibited 2,2-diphenyl-1-picrylhydrazyl (DPPH) radical-scavenging activity and antimicrobial activities against Gram-positive (*Bacillus cereus*) and Gram-negative bacteria (*Klebsiella pneumonia*). Therefore, the plant-mediated biosynthesized ZnNPs can be considered a promising candidate as an antioxidant and antimicrobial agent against pathogenic microbes found in different areas such as food safety and agriculture. Through the utilization of bioinformatics, we identified six potential targets for drug development in *K. pneumonia* and *B. cereus*, along with their corresponding interacting residues with zinc oxide nanoparticles. Additionally, our research revealed that the zinc oxide nanoparticles exhibited binding capabilities with the sulfiredoxin domain located at the specific targets of *K. pneumonia*, a crucial mechanism responsible for the repair of bacterial cells under oxidative stress.

Keywords: zinc nanoparticles; antimicrobial; antioxidant; green synthesis; plant extract

Citation: Abdelmoteleb, A.; Valdez-Salas, B.; Beltran-Partida, E.; Mendez-Trujillo, V.; González-Mendoza, D.; Tzintzun-Camacho, O.; Roumia, A.F. Biosynthesis of Zinc Oxide Nanoparticles Using Garlic Peel Extract and Their Antibacterial Potential. *Microbiol. Res.* **2024**, *15*, 1655–1669. https://doi.org/10.3390/microbiolres15030110

Academic Editor: Juan Ayala

Received: 29 July 2024
Revised: 15 August 2024
Accepted: 21 August 2024
Published: 23 August 2024

1. Introduction

The unique characteristics of nanomaterials contribute to the swift advancement of nanotechnology and nanoscience. Due to their increased surface-to-volume ratio, which alters their physical and biological properties, nanoparticles have improved reactivity, chemical stability, and thermal conductivity [1]. In particular, metal oxide nanoparticles are the most attractive for the scientific community due to their distinctive characteristics, including their catalytic activity, high photostability, high chemical stability, higher conductivity, broad range of radiation absorption, easy availability, inexpensiveness, nontoxicity, and antimicrobial activity properties [2]. The most favored kind of metal oxide-based

nanomaterial are zinc oxide ones; this is due to their unique features such as their strong catalytic activity, their ability to be used in semiconductors with a large surface area, the fact they absorb and filter UV rays, and their biocompatible, antitumor, antibacterial, antioxidant, safe, and nontoxic properties according to the U.S Food and Drug Administration (USFDA) [1,3,4]. Thus, zinc oxide nanoparticles (ZnO NPs) have unique features that has led to their applicability in several areas, including electronics, agriculture, optics, cosmetics, pharmaceuticals, and food [4].

Chemical and physical processes have been used for the manufacturing of ZnO NPs which has led to large manufacturing rates with controllable sizes [5]. The chemical approach involves the use of dangerous and toxic compounds, which negatively impacts animal and human health and leads to environmental pollution, while the physical technique consumes a lot of energy, heat, and pressure [2,6]. Furthermore, the biological and clinical applications of chemically produced ZnO NPs are limited due to their toxicity and decreased biocompatibility, and they can attach to or remain in the final NP products, thus impeding biological uses [4]. Therefore, the development of bio-safe, nontoxic, biocompatible, economical, and environmentally friendly ZnO NPs as a replacement is required. Employing plants or plant components for the biosynthesis of metallic NPs is known as the green synthesis or biosynthesis of NPs, as opposed to the employment of hazardous items that affect the environment [7]. Recently, the green synthesis of ZnO NPs has gained attention as an alternative to chemically and physically produced ZnO NPs without altering their properties. This process employs a variety of bioactive compounds from plants as reductants and stabilizers [6]. This method is cost-effective, less toxic, and eco-friendly in comparison with other synthetic methods [5,7]. It has been reported that a variety of plant extracts have been successfully used in the synthesis of ZnO NPs [8–11].

Because of the excessive use of current antimicrobial drugs, pathogenic bacteria have developed a resistance to existing antibiotics, thus leading to the emergence of new non-response to existing drug strains. Therefore, the search for an alternative, potent, and more effective antimicrobial is considerably urgent [12]. ZnO nanoparticles have garnered significant attention lately because of their remarkable pharmacological characteristics, which include antimicrobial, antioxidant, and anti-cancer effects [4,5]. ZnO NPs have strong antibacterial properties against a variety of microbes and may inhibit the production of biofilms [3]. ZnO NPs exhibit an antimicrobial effect by directly adhering to cell walls or indirectly producing reactive oxygen species (ROS) when exposed to biological fluids or moisture leading to oxidative stress, which disturbs enzymatic activity, microbial membranes, functions, and replication, inhibiting microorganisms [5]. Oxidative stress occurs in biological systems when the highly reactive radical species are overproduced. All biosystems depend on antioxidants to function properly. ZnO NPs have exhibited antioxidant and free-radical scavenging properties in biological systems [12].

Subtractive proteomics is a method which involves the removal of proteins essential to the pathogen's survival but not present in the host [13]. This approach is crucial for identifying druggable proteins that can be considered for therapeutic development. These selected druggable proteins can be used to develop chimeric-subunit or multi-subunit vaccines, which have proven to be an effective treatment option for the control of diseases caused by the pathogen [14]. Once shortlisted, these candidates can be cloned and over-expressed in *E. coli* before being purified using affinity chromatography. Their immunogenicity can then be validated through in vivo testing in suitable animal models. In addition to essential proteins, virulence factors and resistance determinants also play a role in the mediation of bacterial attachments, which can contribute to the pathogenicity of the bacterium [15]. Cytoplasmic proteins are typically targeted for small molecule drug development, while membrane or secreted proteins are more often considered for vaccine development [16].

The objective of the present study was to biosynthesize ZnO NPs by using garlic peel extract and characterize them by carrying out several characterizing analyses. The potential antibacterial effects of the biosynthesized ZnO NPs were examined against the Gram-positive *Bacillus cereus* and Gram-negative bacteria *Klebsiella pneumonia* using the

disc diffusion method. Moreover, the antioxidant activity of ZnO NP biosynthesis was investigated. Likewise, this work focused on identifying druggable essential and virulent proteins from different strains of *Klebsiella pneumoniae* and *Bacillus cereus*, then determining the interaction residues of these targets with zinc oxide nanoparticles. By doing so, we hope to gain a better understanding of the bacteria's molecular mechanisms and identify potential targets for therapeutic intervention.

2. Materials and Methods

2.1. Preparation of Garlic Peel Extract

Garlic skins were collected and washed thrice under tap water to eliminate dust particles; then, they were rinsed using distilled water. The cleaned garlic skins were dried in the oven for one week at 40 °C and then powdered by a grinder mixer (WF-20B, Guangzhou, China). The plant extract was prepared by soaking 25 g of dried garlic skin powder in 250 mL of deionized water inside a 500 mL Erlenmeyer flask. The solution was stirred on a magnetic stirrer at 150 rpm for 24 h. The crude extract was filtered using filter paper (Whatman No. 1) and then centrifuged at 3000 rpm for 10 min at room temperature. The supernatants were collected and passed through a Millipore filter with a 0.45 µm pore size and stored at 4 °C.

2.2. Synthesis of Phytonanoparticles

First, 250 mL of a 0.01 M zinc sulfate ($ZnSO_4$) solution was prepared using distilled water, and an aqueous extract of garlic skin was used to synthesize ZnO NPs. For the synthesis of ZnO NPs, 40 mL of garlic skin extract was mixed with 160 mL of a 0.01 mM zinc sulfate solution. The reaction mixture was incubated in the water bath at 60 °C for 30 min. The change in the reaction mixture's color after the incubation time confirmed the formation of ZnO NPs [17]. The synthesized ZnO NPs were collected by centrifugation at 10,000 rpm for 10 min and washed several times with distilled water. The pellet was dried and kept in sealed bottles for further studies.

2.3. UV–Visible Spectroscopy and Dynamic Light Scattering (DLS) Analysis

UV–vis spectrophotometry was employed for the preliminary characterization of green-synthesized ZnO NPs. The reduction of Zn ions to a nanostructure was examined using a UV–visible spectrophotometer (Thermo Scientific BioMate 3 Spectrophotometer, Waltham, MA, USA), and the absorption spectra were recorded between 250 and 700 nm. A zinc sulfate solution served as a blank solution. The fundamental idea behind UV–vis spectroscopy depends on the electrons' excitation. When a molecule is exposed to UV or visible light, its electrons transit from a lower to a higher energy orbit [18]. On the other hand, the size distribution of the synthesized ZnO NPs was analyzed by dynamic light scattering (DLS) using a Nanotrac wave instrument particle size analyzer (Microtrac, York, PA, USA). ZnO NPs were diluted using deionized water and vortexes before being sampled in the cuvette of the DLS device. The size of the nanoparticles was measured between 0.1 and 1000 µm at 25 °C and a 90° scattering angle [18].

2.4. Scanning Electron Microscopy (SEM) and Energy-Dispersive X-ray Spectroscopy (EDS)

A scanning electron microscope (SEM) (JEOL 6010L; JEOL, Tokyo, Japan) was used to analyze the morphological characteristics of synthesized ZnNPs. For the SEM analysis, the synthesized ZnO NPs were centrifuged at 10,000 rpm for 10 min and dried. The sample film was prepared using a carbon-coated grid to take the sample drop. The film was left to dry before being examined using the SEM grid. The image and size of ZnO NPs were obtained by subjecting the dried sample to an electron beam. An energy-dispersive X-ray spectroscopy (EDS) analysis was performed to detect the elemental composition and the purity of the green-synthesized ZnO NPs. Also, the atomic weights of atoms found in the nanoparticles were confirmed.

2.5. Fourier Transform Infrared Spectroscopy (FTIR)

An FTIR analysis was performed to identify the phytochemicals present in the plant extract, which are responsible for the synthesis of nanoparticles. These substances are in charge of reducing zinc ions as well as stabilizing ZnNPs. FTIR was used to detect the functional groups of both plant extract and ZnO NPs [1]. The spectrum was obtained using the infrared spectroscopy technique. Using this approach, the functional groups contained in garlic skin extract and ZnO NPs were investigated in the 4000–400 cm^{-1} spectrum range.

2.6. Antioxidant and Antibacterial Activity of Biosynthesized ZnO NPs

The determination of the antioxidant activity of the produced ZnO NPs was performed by the 2,2-diphenyl-1-picrylhydrazyl (DPPH) method [11]. A DPPH solution (100 µM) was prepared in 99.9% methanol, and the DPPH scavenging activity was conducted by mixing 1 mL of ZnO NP samples, $ZnSO_4$, and ascorbic acid (standard) at different concentrations (25, 50, 100, 200, 400, and 600 µg/mL) with 3 mL of freshly prepared DPPH solution. The mixture was incubated at ambient temperature for 30 min in the dark. After the incubation time, a UV–visible spectrophotometer was used to measure the decrease in the DPPH radical by measuring the absorbance at 517 nm. The DPPH scavenging activity of the synthesized ZnO NPs was calculated using the following equation:

$$\% \text{ of DPPH inhibition} = \left(\frac{A0 - As}{A0}\right) \times 100$$

where A0 refers to the control reading, and As refers to the sample reading at 517 nm to determine the percentage of inhibition.

In addition, the effect of the extract on the antibacterial activity of the synthesized ZnO NPs, garlic skin extract, and zinc sulfate solution was assessed against Gram-positive bacteria *Bacillus cereus* and Gram-negative *Klebsiella pneumonia*. The antibacterial activity was determined by using the disc diffusion method. In brief, 1 mL of each bacterial strain (1.6×10^7 CFU/mL) was inoculated separately onto individual nutrient agar plates. Six-millimeter sterilized filter paper discs were individually soaked in ZnO NPs, garlic skin extract, and zinc sulfate solution and allowed to dry. Discs socked in sterile distilled water served as control. Four discs (one for each treatment) were transferred into each bacterial strain plate. The experiments were performed in triplicates and incubated at 35 ± 2 °C for 24 h. After that, the formation of inhibition zones around the discs was observed and measured in millimeters in all plates.

2.7. In Silico Analysis

An investigation was undertaken to evaluate the efficacy of zinc oxide nanoparticles through molecular docking simulations. This study was built upon two main axes: (1) a subtractive proteomic approach to identify probable drug targets in both pathogenic organisms, and (2) molecular docking of zinc oxide nanoparticles with the detected drug targets.

2.7.1. Subtractive Proteomic Analysis

To obtain the available proteomes of *K. pneumoniae* and *B. cereus*, the Uniprot (Uniprot 2024_02) "https://www.uniprot.org/ (accessed on 2 June 2024)" was utilized. Sequences were first reduced in redundancy using MMSEQ2 [19], and sequences shorter than 100 residues were removed. Proteins from the respective proteomes were then compared to those of *Homo sapiens* using Blastp, with an e-value threshold of 0.0001. Proteins without hits to *H. sapiens* proteins were further analyzed. A Blastp analysis was conducted for these proteins against human gut flora [20,21], with an e-value threshold of 0.0001 for identifying proteins without hits to gut flora. VFDB was used for further analysis, with an e-value threshold of 0.00001. The members with VFDB hits were then compared to DEG db using an e-value threshold of 0.00001. DeepLoc (v. 2.0) [22,23] was employed to predict the subcellular location of the members with DEG db hits. Cytoplasmic proteins with hits

to DEG were subjected to a druggability analysis comparing them to TDD and ChEMBL (V.31), using Blastp with an e-value threshold of 0.00001 [24,25]. Then, AntigenPro "http://scratch.proteomics.ics.uci.edu. (Accessed on 3 June 2024)" was accessed to detect the probable antigens with a cutoff 0.5 [26]. Finally, a Pfam screening was conducted using hmmscan to determine if the targets had known domains [27].

2.7.2. Molecular Docking Simulation

All the files obtained from Alphafold were acquired in PDB format as reported by Jumper et al. [28]. Subsequent to the acquisition of all the pertinent files, the next step involved the preparation and design of zinc oxide nanoparticles (ZnO NPs). During this phase, zinc oxide nanostructures with specific dimensions of $X \times Y \times Z = 5 \times 5 \times 5$ angstroms were synthesized utilizing Biovia Materials Studio, Release 2020 software. The process of molecular docking was executed by employing AutoDock Vina 1.2.0, a software tool developed by Eberhardt et al. [29]. The visualization of protein–ligand interactions was performed using the Pymol software package (v1).

2.8. Statistical Analysis

The findings were statistically analyzed using SPSS version 21 software and compared using one-way ANOVA and Tukey post hoc test ($p < 0.05$). The results were acquired in triplicates and expressed as mean ± standard deviation (SD).

3. Results and Discussion

3.1. Biosynthesis of ZnO NPs Using Garlic Peel

The phytochemicals in plant extracts play a crucial role in the eco-friendly and safe biosynthesis of ZnO NPs, which act as reducing and capping agents for Zn ions to ZnO NPs. The metabolites in extracts of garlic (*Allium sativum* L.) peel include tannins, flavonoids, and phenolic compounds [30]. During the biosynthesis process of ZnO NPs, zinc ions (Zn^{2+}) are obtained from the precursor in the reaction mixture and reduced from Zn^{2+} to Zn^{0} by bioactive compounds in plant extracts such as flavonoids, phenols, and tannins by providing electrons in a redox process to Zn^{2+} ions. This starts the nucleation of ZnO NPs and their subsequent growth. Furthermore, these phytochemicals bind to the surface of NPs, inhibit agglomeration, and maintain the stability of colloidal solutions, thereby acting as both reductants and stabilizers of NPs [2,5]. The biosynthesis of ZnO NPs using plant extracts could be explained by the plants' capacity for metal ion bioaccumulation and the role of active phytoconstituents which act as bioreductants and stabilizers [31]. Similarly, the biosynthesis of zinc oxide nanoparticles using plant extracts such as *Eucalyptus globulus* Labill. leaf [2], *Abronia villosa* [8], *Sambucus ebulus* leaf [9], and garlic skin [17] have been reported previously. In this sense, the synthesized ZnO nanoparticles were characterized through the utilization of absorption spectra derived from UV spectroscopy. ZnO NPs have a distinctive broad absorption peak that ranges from 300 to 400 nm [32]. A UV–vis spectroscopy analysis for ZnO nanoparticles biosynthesized using garlic peel extract and zinc sulfate precursor exhibited a distinctive absorption peak at 365 nm, which preliminary confirmed the formation of ZnO NPs (Figure 1). The particle size reduction caused the adsorption edge to shift to a lower wavelength [33]. In this context, biosynthesized ZnNPs using clove buds exhibited an absorption peak at 374 nm when exposed to UV radiation [32]. The absorption of ZnO NPs is influenced by several variables, including the structure and size of nanoparticles, the band gap, the surface nature, oxygen shortage, the shape, and impurity centers. These variables may have an impact on the absorption peak's blue shift as a result of the decrease in particle size [33]. The significant absorption of ZnO NPs in the UV spectrum suggests that they can be used in medical applications like antibacterial ointments or sunscreen protectors {31]. Similar investigations revealed that ZnO nanoparticles had an absorption band between 355 and 380 nm [33].

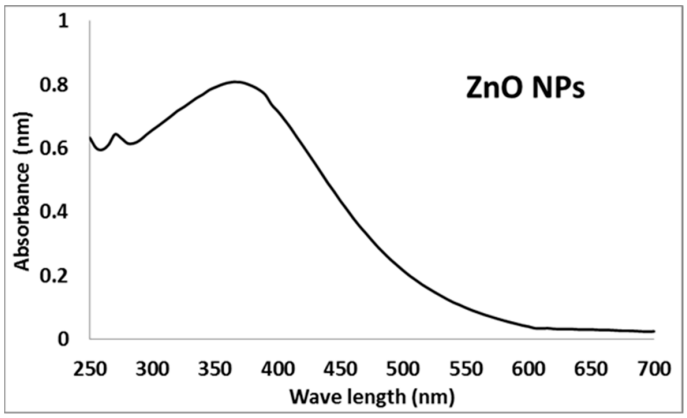

Figure 1. UV–vis spectrum of ZnO NPs biosynthesized from garlic peel extract.

3.2. Scanning Electron Microscopy (SEM) and Energy-Dispersive X-ray Spectroscopy (EDS)

The morphological characterization of biosynthesized ZnO NPs was conducted by SEM analysis. SEM determines crucial characteristics of ZnO NPs such as distribution, aggregation, surface morphology, and size of nanoparticles [34]. Figure 2 illustrates the morphological characteristics of the green obtained ZnO NPs using garlic peel extract, which were irregular. On the contrary, the SEM result of biosynthesized ZnO NPs using *Acacia catechu*, *Artemisia vulgaris*, and *Cynodon dactylon* extracts exhibited the formation of spherical-shaped ZnO nanoparticles [5]. The SEM analysis exhibited a slight agglomeration that indicated the distinct characteristics of biosynthesized ZnO NPs using plant extract [11]. This is because green-synthesized NPs have a larger surface area and a persistent affinity for one another, which leads to agglomeration or aggregation [2]. The agglomeration of biosynthesized nanoparticles (NPs) can be caused by phytochemical moieties found on the surface of the particles, polarity, electrostatic attraction, and high surface area, or it can be ascribed to different factors such as changes in temperature and medium pH during the synthesis process [5,10]. An EDS analysis was performed to verify the existence of Zn and oxygen, their relative abundance, the elemental composition, and the existence of impurities in the biosynthesized nanoparticles [34].

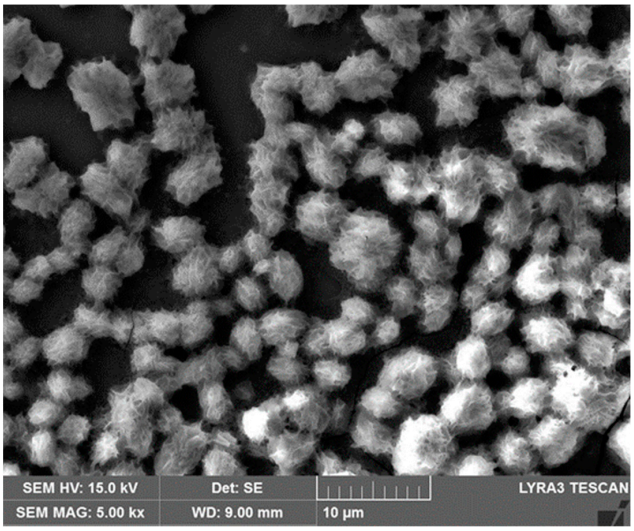

Figure 2. SEM image of garlic peel extract-mediated biosynthesized ZnO NPs.

The EDS analysis showed that the biosynthesized structure contained the desired elemental composition of both zinc and oxygen along with impurities such as Ca, Na, K, Cl, S, Si, Mg, and C. The presence of these extra components can be attributed to the different metabolites that are found in the plant extract [5]. The presence of zinc in oxide form was

verified by detecting the Zn and O peaks. The spectrum exhibited Zn and O peaks between 0 and 2 KeV, and another Zn peak was detected between 8 and 10 KeV (Figure 3). Similar results were reported in previous studies [2,5,35].

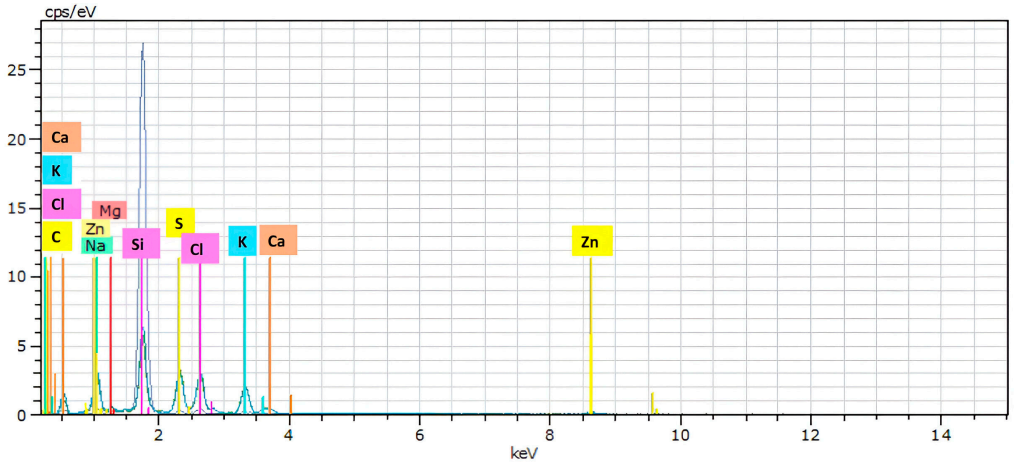

Figure 3. EDX of ZnO NPs produced by using garlic peel extract.

3.3. DLS and FTIR Analysis

A DLS analysis was used to detect the size, polydispersity index, and size distribution in the colloidal suspension of nanoparticles [36]. Figure 4 illustrates the mean nanoparticle size dispersion of ZnO NPs suspension. The analysis showed that the size of green-synthesized ZnO NPs in the colloidal suspension ranged from 7 to 47 nm, and the average size of biosynthesized nanoparticles was 17 nm. The graph clearly showed that the ZnO NP suspension had different sizes of biosynthesized nanoparticles. The variation in the biosynthesized ZnO NPs' size may be ascribed to the existence of carbohydrates, proteins, and enzymes that participate in the synthesis and capping of nanoparticles through various mechanisms [37]. In this context, the size of ZnO NPs synthesized using *Cymbopogon citratus* extract ranged from 20 to 24 nm [7]. On the other hand, the FTIR analysis provided molecular details about the biomolecules and molecules contained in the plant extracts that took part in the manufacturing of the nanoparticles by assisting in the identification of the functional groups that existed in the compounds on the surface of the nanomaterial. The FTIR analysis conducted for this investigation was within the spectrum region of 4000 to 400 cm^{-1}.

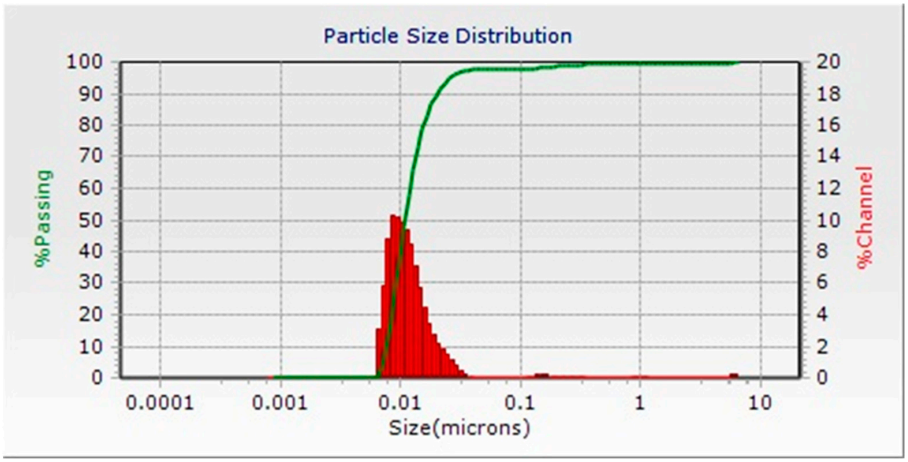

Figure 4. Size distribution of biosynthesized ZnO NPs from DLS.

Figure 5 displays the IR spectra of the plant extract and the biosynthesized nanoparticles. The FTIR analysis demonstrated the presence of various functional groups derived

from plant extracts, which play a vital role in the biosynthesis of ZnO NPs by acting as reducing and capping compounds. Generally, the FTIR spectrum analysis of both garlic peel extract and the biosynthesized ZnO NPs using garlic peel extract exhibited similar peaks at different wavenumbers. The observed peaks in the range of 3000–3700 cm^{-1} generally indicate the existence of the O-H stretch bond of free hydroxyl groups [3].

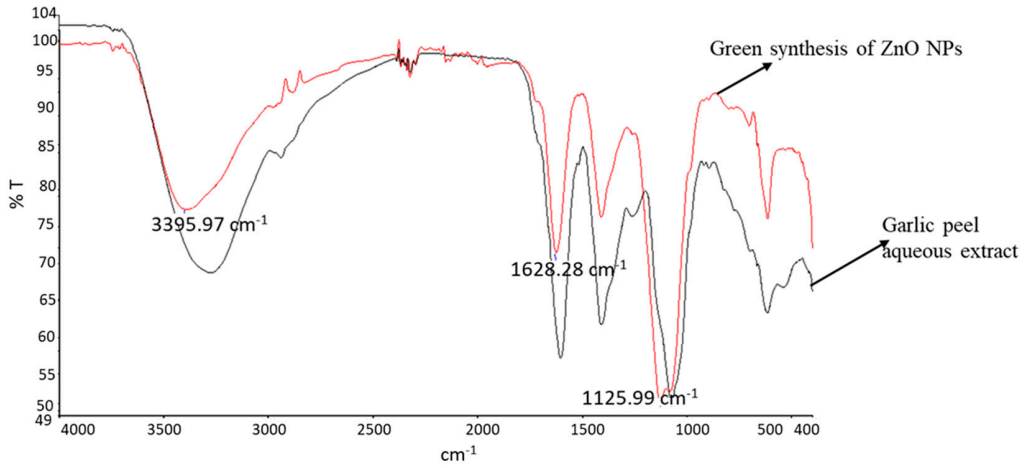

Figure 5. FTIR spectra of garlic peel aqueous extract and biosynthesized ZnO NPs.

As illustrated in Figure 5, a strong peak was observed at 3395 cm^{-1}, which confirmed that garlic peel extract contained alcohol, polyphenols, and flavonoid functional groups that contain various hydrogen bonds. The vibration frequency of each bond type found in the FTIR investigation varied. The peak at 1625 cm^{-1} showed a carbonyl group (C=O) stretching vibration, which signified ketone and aldehyde functionality. The medium absorbance at around 1412 cm^{-1} was related to the O-H bending of alcohols. Another peak at around 1125 cm^{-1} was linked to the C-O stretch of carboxylic acids, tertiary alcohol, and esters. As shown in Figure 5, the observed peaks in the range of 400–600 cm^{-1} were typically associated with the metal–oxygen interaction [5]. Specifically, the presence of a peak at around 418 cm^{-1} signified the Zn–O bond's stretching vibration, confirming the presence of ZnO NPs. Therefore, the result revealed the presence of alcohol, polyphenols flavonoids, ketone, aldehydes, carboxylic acids, and esters in garlic peel extract, which play a crucial role in the biosynthesis process of ZnO NPs. In green synthesis, the mechanism of donor–acceptor was employed to reduce Zn^{+2} ions. Electrophile zinc complexes received an electron from the hydroxyl or oxygen molecules in the garlic peel extract, which reduced zinc ions and oxidized O-H groups [9,11]. The FTIR result exhibited the presence of metabolites, like polyphenols, alkaloids, carboxylic acid, and flavonoids, which were chained to ZnO NPs. These compounds, especially phenolic, and flavonoids, contributed to the conversion of Zn^{+2} ions into ZnO NPs. Also, carboxylic groups found in plant extract appeared to interact with the Zn surface and stabilize ZnO NPs [11,31]. According to FTIR data, the existence of several functional groups including bioactive substances in the garlic peel extract made the biosynthesis technique successful and effective.

3.4. Antibacterial Activity of Synthesized Metal Oxide Nanoparticles

An antibacterial assay was performed by the disc diffusion technique to evaluate the inhibitory effect of biosynthesized ZnO NPs against Gram-positive (*Bacillus cereus*) and Gram-negative bacteria (*Klebsiella pneumonia*). The antimicrobial activity of the synthesized nanoparticles was observed as an inhibition zone around the discs of ZnO NPs that prevented bacterial growth. The biosynthesized ZnO NPs exhibited remarkable inhibition zones against both Gram-positive and Gram-negative bacteria (Figure 6). The discs of biosynthesized ZnO NPs from garlic peel extract showed inhibition zones with radial diameters of 13 ± 2.6 and 15 ± 1.7 mm against *Bacillus cereus* and *Klebsiella pneumonia*,

respectively. No inhibition zones were recorded around the discs of the control (distilled water), aqueous extract of garlic peel, and zinc sulfate against both Gram-positive and Gram-negative bacteria. These findings suggested that the biosynthesized ZnO NPs had a notable antibacterial effect against both Gram-positive and Gram-negative bacteria classes. ZnO NPs obtained using *Pisonia alba* leaf extract showed antibacterial activity with 20.4 and 11 mm inhibition zones against *Staphylococcus aureus* (Gram-positive) and *Klebsiella pneumoniae* (Gram-negative), respectively [6].

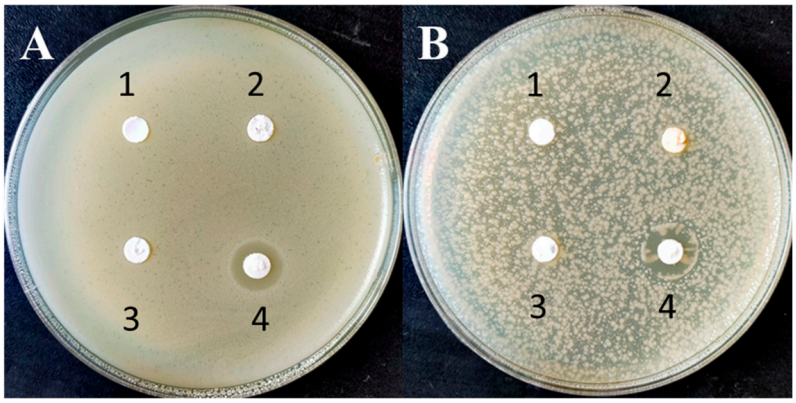

Figure 6. Antibacterial activity of biosynthesized ZnO NPs against *Bacillus cereus* (**A**) and *Klebsiella pneumonia* (**B**), negative control (1), plant extract (2), zinc sulfate (3), ZnO NPs (4).

Although the exact antimicrobial mechanism of zinc oxide nanoparticles is still not well known, research has revealed that the inhibitory effect of ZnO NPs on microorganisms can be attributed to the destruction of DNA and proteins, intracellular content leakage across membranes, toxic ion release, and the formation of reactive oxygen species (ROS) [38,39]. Because ZnO NPs have a vast surface area, they may be able to make better contact with microbes, which has demonstrated effective antibacterial properties. After that, the released zinc ions may bind to DNA molecules and cause cross-linking inside and between nucleic acid strands, disrupting the double helix.

The existence of zinc ions within bacterial cells leads to the disturbance of metabolic processes [40]. The food and drug administration (FDA) views zinc oxide as generally safe. Zinc oxide nanoparticles are used in many fields, including in industry, medicine, food science (preservatives), and textiles. They are also used as drug delivery agents in pharmaceutical fields [3]. Smaller NPs are thought to have a stronger surface reactivity, which allows them to permeate cells effortlessly releasing free Zn^{2+} from ZnO NPs, which is one probable antibacterial mechanism. A primary antibacterial process involves the release of Zn^{2+} ions on biomolecules, such as proteins, enzymes, and DNA, present in bacterial cells. Numerous bacterial cell processes, including metabolism, active transport, and enzyme activity, are known to be disrupted by the produced ZnO NPs, which ultimately leads to bacterial cell death [41]. ZnO NPs commonly exploit the generation of reactive oxygen species (ROS) like hydrogen peroxide (H_2O_2), hydroxyl ion (OH), and superoxide anion (O_2) during exposure to UV radiation to induce oxidative stress and cell death in bacteria [42]. These ROS are produced when hydroxyl groups on the surface of nanoparticles react with water (H_2O) to form hydroxyl radicals (OH^-) and hydrogen ions (H^+), which subsequently generate superoxide anion (O_2^-) in the existence of oxygen (O_2) [4]. Eventually, H_2O_2 penetrates the bacterial cell membrane barrier, destroying cellular components such as proteins, lipids, and DNA causing cell injury and death [4]. Additionally, the antibacterial activity of biosynthesized ZnO NPs could be ascribed to the existence of carboxyl and amine groups on their cell surface, and the great affinity of ZnO ions toward these groups [40]. The antibacterial activities of plant-mediated biosynthesized ZnO NPs against pathogenic bacteria have been reported in previous studies [6,40]. Due to their potent antibacterial activity, stability in harsh environments, and minimal toxicity

to humans, zinc oxide nanoparticles are among the most investigated inorganic metal oxide nanoparticles [3]. In this context, the biosynthesized ZnO NPs using extracts of *Artemisia vulgaris*, *Acacia catechu*, and *Cynodon dactylon* possess a promising potential for use in biomedical applications [5]. However, ZnO nanoparticles' safety for human health is still doubted and needs more investigation.

3.5. Antioxidant Activity of Biosynthesized ZnO NPs

The antioxidant activity of the garlic peel extract-mediated biosynthesized ZnO NPs was estimated through the DPPH scavenging assay. The DPPH assay is typically predicated on the reduction in the DPPH moiety following its acceptance of an electron from a donor species and forming a bright yellow molecule of diphenyl picrylhydrazine [35]. In the current study, the DPPH radical scavenging experiment was performed in vitro to evaluate the antioxidant capability of the biosynthesized ZnO NPs. The color shift in the DPPH solution from deep violet to pale yellow indicates the radical scavenging capacity of both biosynthesized ZnO NPs and standard ascorbic acid, where the antioxidants found in the biosynthesized ZnO NPs reduce the stable nitrogen radical in the DPPH solution, resulting in a decrease in the absorbance at 517 nm [35]. According to the findings illustrated in Figure 7, the biosynthesized ZnO NPs effectively prevented free radicals, and the effectiveness of the nanoparticles increased along with their concentration. The inhibitory percentage of biosynthesized ZnO NPs increased gradually and achieved a maximum of 87% at its greatest concentration (600 µg/mL). The radical scavenging capacity of biosynthesized ZnO NPs was lower than that of ascorbic acid (standard) and higher than that of zinc sulfate at all concentrations. Similarly, zinc oxide nanoparticles synthesized using tuber extract of *Coccinia abyssinica* displayed a free-radical scavenging capacity with a maximum of about 70% scavenging activity at 800 µg/mL of ZnO NPs [12]. The free radical that is located at the nitrogen atom in DPPH reduces to hydrazine by receiving the electron density from ZnO NPs. Additionally, the several phytochemicals adhered to the surface of nanoparticles may play an important role in the biosynthesized ZnO NPs' antioxidant activity [4]. Previous research has documented comparable effects of biosynthesized ZnO NPs as potent antioxidants [4,11,35]. As a result, the antioxidant assay revealed that the biosynthesized ZnO NPs had promising antioxidant activities and might find application in the pharmaceutical sector.

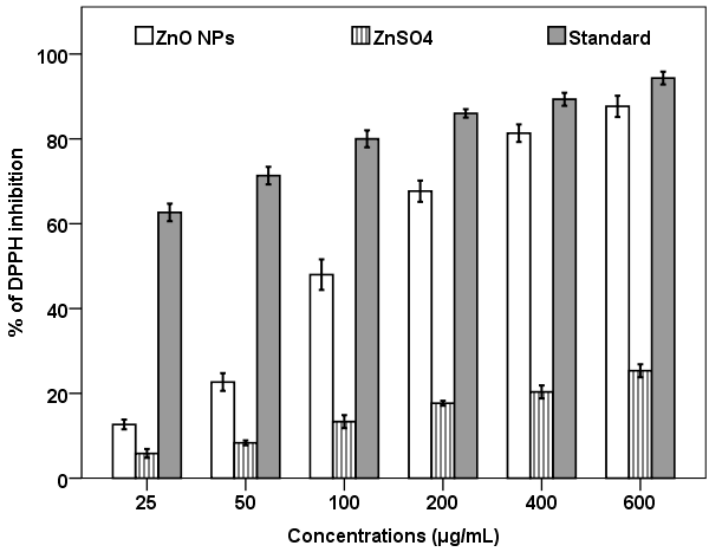

Figure 7. DPPH free-radical scavenging assay of the biosynthesized ZnO NPs and $ZnSO_4$.

3.6. In Silico Analysis

From the Uniprot database, a total of four proteomes were retrieved for *K. pneumoniae* and three for *B. cereus*, as shown in Table 1. A subtractive proteomic analysis was conducted

for each organism, resulting in the identification of three targets that exhibited essentiality and virulence, exclusive presence in the respective pathogen, and absence in both human and gut microbiota. Furthermore, these identified targets have not been subjected to treatment with any known drug compounds.

Table 1. The proteomes of *K. pneumonia* and *B. cereus*.

Organism	Proteome ID	Tax ID	Protein Count	Target No.
B. cereus	UP000000594	1392	5493	1
	UP000027822	574376	4374	0
	UP000220020	64104	5787	0
	UP000001417	226900	5240	2
K. pneumonia	UP000007841	1125630	5728	1
	UP000255382	574	6726	2
	UP000326328	2590872	48	0

The data presented in Table 2 showcase the structural attributes of the predicted drug targets in both organisms and their binding affinity with zinc oxide nanoparticles. All detected targets exhibited an antigenic capacity based on the Anigenpro prediction. In general, the candidates from *B. cereus* displayed a lower binding affinity with zinc oxide nanoparticles compared to the candidates from *K. pneumonia*. The candidates from *B. cereus* lacked known domains in Pfam, while the three candidates from *K. pneumonia* exhibited a conserved sulfiredoxin (Srx) domain (PF02195). It is worth noting that the nanoparticles of zinc oxide interacted exclusively with this domain (Figure 8).

Table 2. Structural characteristics of the predicted drug targets.

Organism	Tax ID	Accession	Pfam	Antigenecity Score	Binding Affinity (kcal/mol)
B. cereus	1392	A0A6L7H1K2	No domains found	0.88	−3.3
	226900	Q818P1	No domains found	0.83	−4.9
	226900	Q81DP8	No domains found	0.72	−4.0
K. pneumonia	1125630	A0A0H3GZ74	PF02195 PF08775	0.76	−5.0
	574	A0A377YWZ3	PF02195 PF08775	0.77	−5.4
	574	A0A377YX32	PF02195 PF18090	0.52	−5.3

When the cell is exposed to oxidative stress, a cluster of proteins known as peroxiredoxins (Prxs), belonging to the peroxidases family (PF10417), participate in the reduction of hydroperoxides. These proteins undergo a reversible oxidation process to sulfinic acid (Cys-SO_2H) during their catalytic activity. In yeast, it has been determined that Srx is accountable for reversing the resulting enzyme inactivation. The process of reducing cysteine sulfinic acids by Srx entails activation through phosphorylation, followed by a reduction step mediated by thiol. The significance of PF02195 lies in its contribution to the antioxidant role of peroxiredoxins. This protein is likely implicated in the restoration of proteins that have undergone modifications involving cysteine sulfinic acid, as well as in pathways related to protein oxidation signaling [43]. Our research speculates that the involvement of zinc oxide nanoparticles was crucial in combatting *K. pneumonia* by inhibiting the Srx domain. Our results challenge the concept of the oxidative inactivation of Prx enzymes in prokaryotes [43], particularly as we observed that *K. pneumonia* (Tax id:573) possessed 29 proteins containing the Prx domain. Therefore, a further exploration is necessary to fully comprehend the oxidative inactivation of prokaryotic Prx enzymes. Given the fact that *B. cereus* candidates lack identifiable domains in Pfam, a multiple sequence alignment (Figure 9) was generated to ascertain potential similarities among these entities.

Remarkably, A0A6L7H1K2 and Q818P1 exhibited a degree of resemblance and interacted with zinc oxide nanoparticles in similar regions (Figure 10), whereas Q81DP8 displayed a lower level of similarity compared to the former two candidates. Our findings fortify the notion of annotating these elusive domains and represent a significant advancement in the quest for therapeutic agents targeting *B. cereus*.

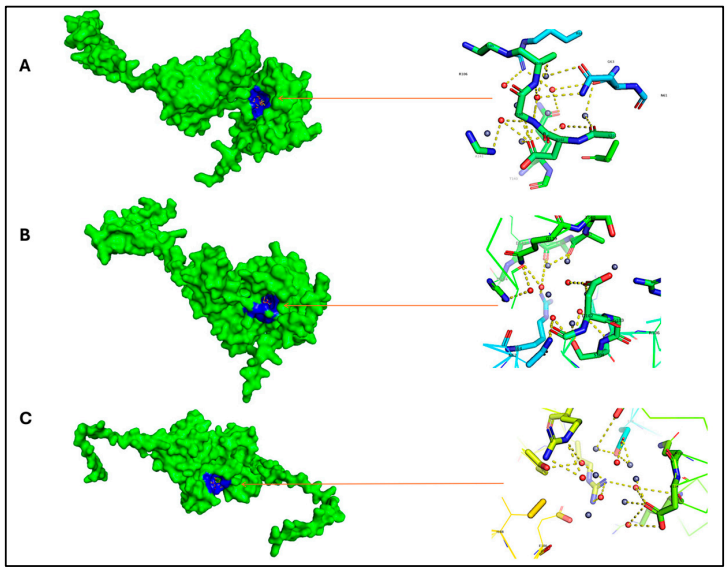

Figure 8. The interactions involved between zinc oxide nanoparticles, the drug targets of *K. pneumonia,* and their interaction residues. (**A**) A0A0H3GZ74 (61ASN, 62ASN, 63GLY, 64ARG, 101LEU, 102ASP, 103GLY, 104SER, 105ARG, 106ARG, 135ALA, 138ILE, 139GLN, 140THR, 141ALA); (**B**) A0A377YWZ3 (62ASN, 64ARG, 101LEU, 102ASP, 103GLY, 104SER, 105ARG, 106ARG, 135ALA, 139GLN, 140THR, 141ALA, 142LYS, 143GLU, 144HIS, 144HIS); and (**C**) A0A377YX32 (78GLU, 150ARG, 153ASN, 154ASP, 158THR, 163ARG, 166ARG, 167TYR, 186GLU, 188ILE). In the 3D models (left side), the whole protein is shown in green while the interaction residues with the ZnO nanoparticles are shown in blue.

```
CLUSTAL O(1.2.4) multiple sequence alignment


tr|Q81DP8|Q81DP8_BACCR             ------------------------------------------------------------       0
tr|A0A6L7H1K2|A0A6L7H1K2_BACAN     MSVKKKTQVRTGKMVRELMLADEDVNASLIMVYSENGVNAEIKIEGLTPKCNEELFLSGN       60
tr|Q818P1|Q818P1_BACCR             MSVKKKTQVRTGKMVRELMLADEDVNASLIMVYSENGVNAEIKIEGLTPKCNEELFLSGN       60


tr|Q81DP8|Q81DP8_BACCR             ------------------------------------------------------------       0
tr|A0A6L7H1K2|A0A6L7H1K2_BACAN     VDWNKSVIYKIVDFTGNAEVGKVTLTAMNKNNVSLEIERVMWSKENKETAEQEETVVEAT       120
tr|Q818P1|Q818P1_BACCR             VDWNKSVIYKIVDFTGNAEVGKVTLTAMNKNNVSLEIERVMWSKENKEAAEQEETQVEAA       120


tr|Q81DP8|Q81DP8_BACCR             ----MLDSYPGHFLPNTEAPTEEEALIALLALGGYDPDNMDGKPLTMESAVEILRK----       52
tr|A0A6L7H1K2|A0A6L7H1K2_BACAN     PKKEVVVEVPKAVTPAPKPVTRVET-PAI-ASTPKPTPAPTPKPVSVEAAVELSTPAPVK       178
tr|Q818P1|Q818P1_BACCR             PKKEVVVEAPKAITPAPKPVTRVET-PAM-A--PKPTPVPTPKPVSVEAAVELVTPAPVK       176
                                       :: . *  . *  :  *. *:  *: *           **:::*:***:


tr|Q81DP8|Q81DP8_BACCR             ----------DGSALASL------EEETILNLKETYVNSVGLLGKYVPKVYNGDILFFRS       96
tr|A0A6L7H1K2|A0A6L7H1K2_BACAN     KAVPTPVTKQETTPVAPVKPKQSALTETNSKLQENYVKLVKK---TIE-----------       223
tr|Q818P1|Q818P1_BACCR             KAVPTPVTKQETAPVAPAKPKQPALTETNSKLQENYVKLVKK---TIE-----------       221
                                             : : :*          **  :*:*.**: *      :


tr|Q81DP8|Q81DP8_BACCR             TVIPDWFDPISPNTWLNYLDGQIVQHDIDCRHKDLCQPGPLTEIGQVLAKYLQ-----NK       151
tr|A0A6L7H1K2|A0A6L7H1K2_BACAN     -VC-----------QDYELGIDIDDSIEGLKEELQSQGISVTFDKEIMDVVNRLRSLQD       270
tr|Q818P1|Q818P1_BACCR             -VC-----------QDYELGIDIDDSIESLKEELQSQGISVTFDKEIMDVVNRLRSLQD       268
                                    *             :*  *  ::..*:  :::* . *  . :.: : . ::     :.


tr|Q81DP8|Q81DP8_BACCR             KGV--SRV----       157
tr|A0A6L7H1K2|A0A6L7H1K2_BACAN     KGIRVEKVLNLL       282
tr|Q818P1|Q818P1_BACCR             KGIKVEKVLNLL       280
                                   **:  .:*
```

Figure 9. Multiple sequence alignment for the drug targets of B. cereus. An asterisk (*) denotes locations that possess a singular, completely conserved amino acid residue; a colon (:) signifies the preservation of similarities among groups exhibiting highly similar characteristics; and a period (.) signifies the preservation of similarities across groups characterized by weakly similar attributes.

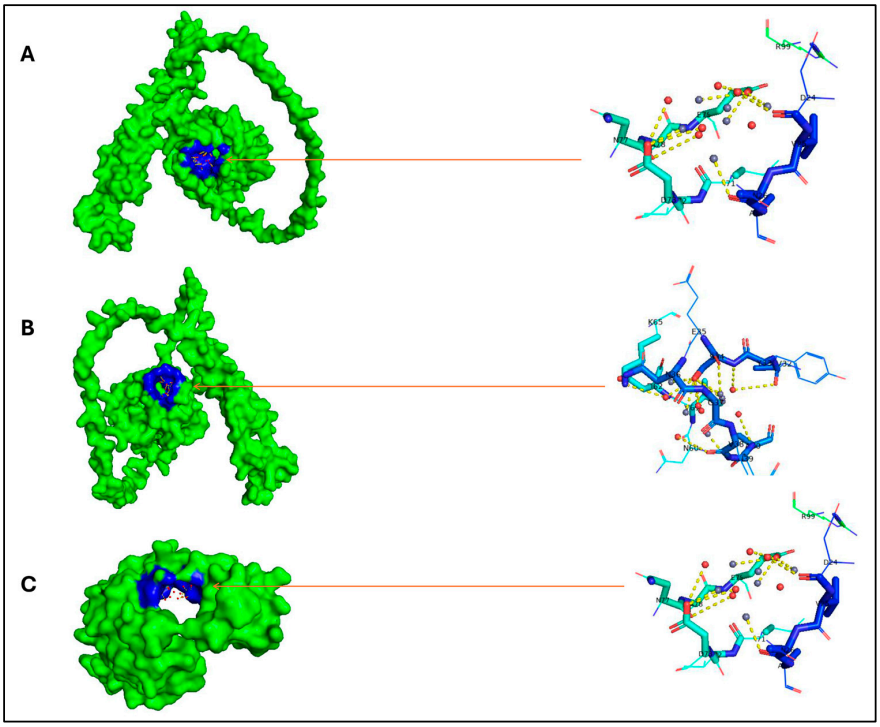

Figure 10. The interactions involved between zinc oxide nanoparticles, the drug targets of *B. cereus*, and their interaction residues. (**A**) A0A6L7H1K2 (24ASP, 25VAL, 26ASN, 27ALA, 71ILE, 72VAL, 73ASP, 77ASN, 78ALA, 79GLU, 99ARG); (**B**) Q818P1 (32VAL, 33TYR, 34SER, 35GLU, 36ASN, 37GLY, 38VAL, 39ASN, 40ALA, 60ASN, 61VAL, 62ASP, 65LYS); and (**C**) Q81DP8 (10LEU, 11PRO, 12ASN, 13THR, 16PRO, 20GLU, 21ALA, 24ALA, 72TYR, 76VAL, 79LEU). In the 3D models (left side), the whole protein is shown in green while the interaction residues with the ZnO nanoparticles are shown in blue.

4. Conclusions

In conclusion, the purpose of this work was to use garlic peel extract to synthesize zinc oxide (ZnO) nanoparticles. An environmentally acceptable substitute for conventional chemical synthesis techniques is the use of garlic peel as a reducing agent, which helps to produce biocompatible nanoparticles and lessen environmental effects. The results demonstrated the biosynthesis of ZnO NPs with a distinct color shift and a UV spectrum absorbance peak at 365 nm. The characterization of biosynthesized ZnO NPs was performed using UV–vis, SEM, DLS, EDX, and FTIR analyses. The UV–vis analysis indicated the biosynthesis of ZnO NPs through the absorption spectrum peak, while SEM images and DLS analysis revealed the spherical shape and the size of the nanoparticles ranging from 7 nm to 47 nm, respectively. The EDX analysis confirmed the presence of Zn and oxygen. FTIR indicated the functional groups of bioactive phytochemicals in the plant extract, which are responsible for Zn ions reduction and nanoparticle stabilization. The biosynthesized ZnO NPs exhibited an antioxidant activity slightly lower than the standard at the higher concentrations. The antimicrobial activity of biosynthesized ZnO NPs was performed by the disc diffusion method. The results revealed that the ZnO NPs from garlic peel extract could inhibit the growth of different pathogenic bacteria such as *Bacillus cereus* (Gram-positive) and *Klebsiella pneumonia* (Gram-negative). The antibacterial effectiveness of bioresource-derived ZnO nanoparticles against both Gram-positive and Gram-negative bacterial strains could potentially open up new avenues for its application in food and medicine, particularly in the development of potential antibacterial medicines. Nevertheless, more research is required to determine the toxicity of these ZnO NPs and to conduct tests that will permit their safe application. Future in vivo studies are required to properly understand their biological activities.

Author Contributions: Conceptualization, B.V.-S. and D.G.-M.; methodology, E.B.-P., V.M.-T. and A.A.; software, A.F.R.; validation, V.M.-T., O.T.-C. and A.A.; formal analysis, A.A. and A.F.R.; writing—original draft preparation, A.A. and V.M.-T.; writing—review and editing, D.G.-M. and B.V.-S. All authors have read and agreed to the published version of the manuscript.

Funding: This research was funded by the Universidad Autonoma de Baja California (grant number 001).

Institutional Review Board Statement: Not applicable.

Informed Consent Statement: Not applicable.

Data Availability Statement: The original data presented in the study are included in the article.

Acknowledgments: This study was supported by Universidad Autonoma de Baja California.

Conflicts of Interest: The authors declare no conflicts of interest.

References

1. Shahid, M.; Ijaz, N.; Shahid, B.; Tufail, T.; Ain, H.B.U.; Hussain, M.; Basharat, S.; Ikram, A.; Al Jbawi, E. *Eucalyptus globulus* Labill. Mediated synthesis of ZnO nanoparticles, their optimization and characterization. *Cogent Food Agric.* **2024**, *10*, 2293332. [CrossRef]
2. Barzinjy, A.A.; Azeez, H.H. Green synthesis and characterization of zinc oxide nanoparticles using *Eucalyptus globulus* Labill. leaf extract and zinc nitrate hexahydrate salt. *SN Appl. Sci.* **2020**, *2*, 991. [CrossRef]
3. Ifeanyichukwu, U.L.; Fayemi, O.E.; Ateba, C.N. Green Synthesis of Zinc Oxide Nanoparticles from pomegranate (*Punica granatum*) extracts and characterization of their antibacterial activity. *Molecules* **2020**, *25*, 4521. [CrossRef]
4. Murali, M.; Gowtham, H.G.; Shilpa, N.; Singh, S.B.; Aiyaz, M.; Sayyed, R.Z.; Shivamallu, C.; Achar, R.R.; Silina, E.; Stupin, V.; et al. Zinc oxide nanoparticles prepared through microbial mediated synthesis for therapeutic applications: A possible alternative for plants. *Front. Microbiol.* **2023**, *14*, 1227951. [CrossRef]
5. Acharya, R.; Tettey, F.; Gupta, A.; Sharma, K.R.; Parajuli, N.; Bhattarai, N. Bioinspired synthesis and characterization of zinc oxide nanoparticles and assessment of their cytotoxicity and antimicrobial efficacy. *Discov. Appl. Sci.* **2024**, *6*, 85. [CrossRef]
6. MuthuKathija, M.; Sheik, M.B.M.; Rama, V. Green synthesis of zinc oxide nanoparticles using *Pisonia alba* leaf extract and its antibacterial activity. *Appl. Surf. Sci. Adv.* **2023**, *15*, 100400. [CrossRef]
7. Mohammed, Y.H.I.; Alghamdi, S.; Jabbar, B.; Marghani, D.; Beigh, S.; Abouzied, A.S. Green synthesis of zinc oxide nanoparticles using *Cymbopogon citratus* extract and its antibacterial activity. *ACS Omega* **2023**, *8*, 32027–32042. [CrossRef]
8. Abdelmoteleb, A.; Valdez-Salas, B.; Beltran-Partida, E.; Gonzalez-Mendoza, D. Green synthesis of silver nanoparticles from *Abronia villosa* as an alternative to control of pathogenic microorganisms. *J. Renew. Mater.* **2020**, *8*, 69–78. [CrossRef]
9. Alamdari, S.; Sasani, G.M.; Lee, C.; Han, W.; Park, H.H.; Tafreshi, M.J. Preparation and Characterization of Zinc Oxide Nanoparticles Using Leaf Extract of *Sambucus ebulus*. *Appl. Sci.* **2020**, *10*, 3620. [CrossRef]
10. Chandrasekar, L.P.; Sethuraman, B.D.; Subramani, M.; Mohandos, S. Green synthesised ZnO nanoparticles from *Plectranthus amboinicus* plant extract: Removal of safranin- o and malachite green dyes and anti-bacterial activity. *Int. J. Environ. Anal. Chem.* **2023**, *26*, 1–18. [CrossRef]
11. Islam, M.F.; Islam, S.; Miah, M.A.S.; Huq, A.K.O.; Saha, A.K.; Mou, Z.J. Green synthesis of zinc oxide nano particles using *Allium cepa* L. waste peel extracts and its antioxidant and antibacterial activities. *Heliyon* **2024**, *10*, e25430. [CrossRef] [PubMed]
12. Safawo, T.; Sandeep, B.; Pola, S.; Tadesse, A. Synthesis and characterization of zinc oxide nanoparticles using tuber extract of anchote (*Coccinia abyssinica* (Lam.) Cong.) for antimicrobial and antioxidant activity assessment. *OpenNano* **2018**, *3*, 56–63. [CrossRef]
13. Kumar Jaiswal, A.; Tiwari, S.; Jamal, S.B.; Barh, D.; Azevedo, V.; Soares, S.C. An in silico identification of common putative vaccine candidates against treponema pallidum: A reverse vaccinology and subtractive genomics based approach. *Int. J. Mol. Sci.* **2017**, *18*, 402. [CrossRef]
14. Lee, N.H.; Lee, J.A.; Park, S.Y.; Song, C.S.; Choi, I.S.; Lee, J.B. A review of vaccine development and research for industry animals in Korea. *Clin. Exp. Vaccine Res.* **2012**, *1*, 18–34. [CrossRef]
15. Mondal, S.I.; Ferdous, S.; Jewel, N.A.; Akter, A.; Mahmud, Z.; Islam, M.M. Identification of potential drug targets by subtractive genome analysis of *Escherichia coli* O157:H7: An in silico approach. *Adv. Appl. Bioinform. Chem.* **2015**, *8*, 49–63. [CrossRef]
16. Hasan, M.D.A.; Khan, M.D.A.; Sharmin, T.; Hasan Mazumder, M.D.H.; Chowdhury, A.S. Identification of putative drug targets in Vancomycin-resistant *Staphylococcus aureus* (VRSA) using computer aided protein data analysis. *Gene* **2016**, *575*, 132–143. [CrossRef] [PubMed]
17. Modi, S.; Fulekar, M.H. Green synthesis of zinc oxide nanoparticles using garlic skin extract and its characterization. *J. Nanostructures* **2020**, *10*, 20–27.
18. Ikram, I.; Zain, M. Assessment of antibacterial and antifungal activity of cream incorporating silver and zinc oxide nanoparticles synthesized via ginger and garlic extract. *J. Xian Med. Univ.* **2023**, *19*, 1135–1158.
19. Hauser, M.; Steinegger, M.; Söding, J. MMseqs software suite for fast and deep clustering and searching of large protein sequence sets. *Bioinform. Oxf. Engl.* **2016**, *32*, 1323–1330. [CrossRef]

20. Shanmugham, B.; Pan, A. Identification and characterization of potential therapeutic candidates in emerging human pathogen *Mycobacterium abscessus*: A novel hierarchical in silico approach. *PLoS ONE* **2013**, *8*, e59126. [CrossRef]
21. Liu, B.; Zheng, D.; Zhou, S.; Chen, L.; Yang, J. VFDB 2022: A general classification scheme for bacterial virulence factors. *Nucleic Acids Res.* **2022**, *50*, D912–D917. [CrossRef]
22. Zhang, R.; Lin, Y. DEG 5.0, a database of essential genes in both prokaryotes and eukaryotes. *Nucleic Acids Res.* **2009**, *37*, D455–D458. [CrossRef]
23. Moreno, J.; Nielsen, H.; Winther, O.; Teufel, F. Predicting the subcellular location of prokaryotic proteins with DeepLocPro. *bioRxiv* **2024**. [CrossRef]
24. Zhou, Y.; Zhang, Y.; Lian, X.; Li, F.; Wang, C.; Zhu, F. Therapeutic target database update 2022: Facilitating drug discovery with enriched comparative data of targeted agents. *Nucleic Acids Res.* **2022**, *50*, D1398–D1407. [CrossRef]
25. Mendez, D.; Gaulton, A.; Bento, A.P.; Chambers, J.; De Veij, M.; Félix, E. ChEMBL: Towards direct deposition of bioassay data. *Nucleic Acids Res.* **2019**, *47*, D930–D940. [CrossRef]
26. Magnan, C.N.; Zeller, M.; Kayala, M.A.; Vigil, A.; Randall, A.; Felgner, P.L. High-throughput prediction of protein antigenicity using protein microarray data. *Bioinform. Oxf. Engl.* **2010**, *26*, 2936–2943. [CrossRef]
27. Mistry, J.; Chuguransky, S.; Williams, L.; Qureshi, M.; Salazar, G.A.; Sonnhammer, E.L.L. Pfam: The protein families database in 2021. *Nucleic Acids Res.* **2021**, *49*, D412–D419. [CrossRef]
28. Jumper, J.; Evans, R.; Pritzel, A.; Green, T.; Figurnov, M.; Ronneberger, O. Highly accurate protein structure prediction with AlphaFold. *Nature* **2021**, *596*, 583–589. [CrossRef]
29. Eberhardt, J.; Santos-Martins, D.; Tillack, A.F.; Forli, S. AutoDock Vina 1.2.0: New Docking Methods, Expanded Force Field, and Python Bindings. *J. Chem. Inf. Model.* **2021**, *61*, 3891–3898. [CrossRef]
30. Dos Santos, P.C.M.; Da Silva, L.M.R.; Magalhaes, F.E.A.; Cunha, F.E.T.; Ferreira, M.J.G.; de Figueiredo, E.A.T. Garlic (*Allium sativum* L.) peel extracts: From industrial by-product to food additive. *Appl. Food Res.* **2022**, *2*, 100186. [CrossRef]
31. Selim, Y.A.; Azb, M.A.; Ragab, I.H.M.; Abd El-Azim, M. Green synthesis of zinc oxide nanoparticles using aqueous extract of deverra tortuosa and their cytotoxic activities. *Sci. Rep.* **2020**, *10*, 3445. [CrossRef] [PubMed]
32. Ahmed, S.; Qasim, S.; Ansari, M.; Shah, A.A.; Rehman, H.U.; Shah, M.N. Green synthesis of zinc nanoparticles and their effects on growth and yield of *Pisum sativum*. *J. King Saud. Univ. Sci.* **2022**, *34*, 102132. [CrossRef]
33. Droepenu, E.K.; Asare, E.A.; Wee, B.S.; Wahi, R.B.; Ayertey, F.; Kyene, M.O. Biosynthesis, characterization, and antibacterial activity of ZnO nanoaggregates using aqueous extract from *Anacardium occidentale* leaf: Comparative study of different precursors. *Beni Suef Univ. J. Basic. Appl. Sci.* **2021**, *10*, 1. [CrossRef]
34. Dawadi, S.; Katuwal, S.; Gupta, A.; Lamichhane, U.; Thapa, R.; Jaisi, S. Current research on silver nanoparticles: Synthesis, characterization, and applications. *J. Nanomater.* **2021**, *2021*, e6687290. [CrossRef]
35. Maheo, A.R.; Vithiya, B.S.M.; Arul Prasad, T.A.; Mangesh, V.L.; Perumal, T.; Al-Qahtani, W.H. Cytotoxic, Antidiabetic, and Antioxidant Study of Biogenically Improvised *Elsholtzia blanda* and Chitosan-Assisted Zinc Oxide Nanoparticles. *ACS Omega* **2023**, *8*, 10954–10967. [CrossRef]
36. Yedurkar, S.; Maurya, C.; Mahanwar, P. Biosynthesis of Zinc Oxide Nanoparticles Using Ixora Coccinea Leaf Extract—A Green Approach. *Open J. Synth. Theory Appl.* **2016**, *5*, 1–14. [CrossRef]
37. Elrefaey, A.A.K.; El-Gamal, A.D.; Hamed, S.M.; El-belely, E.F. Algae-mediated biosynthesis of zinc oxide nanoparticles from *Cystoseira crinite* (Fucales; Sargassaceae) and it's antimicrobial and antioxidant activities. *Egypt. J. Chem.* **2022**, *65*, 231–240. [CrossRef]
38. Niño-Martínez, N.; Salas Orozco, M.F.; Martínez-Castañón, G.A.; Torres Méndez, F.; Ruiz, F. Molecular mechanisms of bacterial resistance to metal and metal oxide nanoparticles. *Int. J. Mol. Sci.* **2019**, *20*, 2808. [CrossRef] [PubMed]
39. Tiwari, V.; Mishra, N.; Gadani, K.; Solanki, P.S.; Shah, N.A.; Tiwari, M. Mechanism of anti-bacterial activity of zinc oxide nanoparticle against carbapenem-resistant *Acinetobacter baumannii*. *Front. Microbiol.* **2018**, *9*, 1218. [CrossRef]
40. Chikkanna, M.M.; Neelagund, S.E.; Rajashekarappa, K.K. Green synthesis of zinc oxide nanoparticles (ZnO NPs) and their biological activity. *SN Appl. Sci.* **2018**, *1*, 117. [CrossRef]
41. Taran, M.; Rad, M.; Alavi, M. Biosynthesis of TiO_2 and ZnO nanoparticles by *Halomonas elongata* IBRC-M 10214 in different conditions of medium. *BioImpacts BI* **2018**, *8*, 81–89. [CrossRef] [PubMed]
42. Rehman, S.; Jermy, B.R.; Akhtar, S.; Borgio, J.F.; Abdul Azeez, S.; Ravinayagam, V. Isolation and characterization of a novel thermophile; Bacillus haynesii, applied for the green synthesis of ZnO nanoparticles. *Artif. Cells Nanomed. Biotechnol.* **2019**, *47*, 2072–2082. [CrossRef] [PubMed]
43. Chang, T.S.; Jeong, W.; Woo, H.A.; Lee, S.M.; Park, S.; Rhee, S.G. Characterization of mammalian sulfiredoxin and its reactivation of hyperoxidized peroxiredoxin through reduction of cysteine sulfinic acid in the active site to cysteine. *J. Biol. Chem.* **2004**, *279*, 50994–51001. [CrossRef] [PubMed]